MDPI

Article

The Characteristics of the Electro-Thermo-Convective Flow of a Dielectric Liquid Analyzed through the Electric Nusselt Number [†]

Dantchi Koulova [1],* , Philippe Traore [2] and Hubert Romat [2]

[1] Institute of Mechanics, Bulgarian Academy of Sciences, 1113 Sofia, Bulgaria
[2] Institut P', Université de Poitiers, ISAE-ENSMA, 86073 Futuroscope Chasseneuil, France; philippe.traore@univ-poitiers.fr (P.T.)
* Correspondence: dantchi@imbm.bas.bg
[†] This paper is an extended version of paper published in the 2019 IEEE 20st International Conference on Dielectric Liquids (ICDL), held in Roma, Italy, 2019.

Abstract: This paper presents a fundamental study of electro-thermo-convective flows within a layer of dielectric liquid subjected to both an electric field and a thermal gradient. A low-conductivity liquid enclosed between two horizontal electrodes and subjected to unipolar charge injection is considered. The interplay between electric and thermal fields ignites complex physical interactions within the flows, all governed by a set of coupled electro-thermo-hydrodynamic equations. These equations include Maxwell, Navier–Stokes, and energy equations and are solved numerically using an in-house code based on the finite volume method. Electro-thermo-convective flows are driven by two dimensionless instability criteria: Rayleigh number Ra and the stability parameter T, and also by the dimensionless mobility parameter M and Prandtl number Pr. The electric Nusselt number (Ne) analogue to the Nusselt number (Nu) in pure thermal problems serves as an indicator to monitor the shift from a thermo- to an electro-convective flow and its eventual evolution into unsteady, and, later, chaotic flow. This change in regime is observed by tracking the electric Nusselt number's behavior as a function of the stability parameter (T), for different values of the non-dimensional parameters (M, Ra, and Pr). The important role of mobility parameter M for the development of the flow is shown. The flow structure during different development stages in terms of the number of convective cells is also discussed.

Keywords: electrodynamics; electro-thermo-convection; dielectric liquids; numerical analysis charge injection

1. Introduction

The combined effects of an electric field and a thermal gradient applied simultaneously to a dielectric liquid containing a space charge lead to very complex physical interactions in the flow. The electroconvection (EC) and electro-thermo-convection (ETC) in dielectric liquids are problems that have been intensively investigated in recent years [1–4]. Their study is essential for applications with electric fields in heat transfer and flow stability control processes, as well as for a thorough understanding of systems subjected to various natural convective forces (atmospheric convection, solar magneto-convection).

The space charge in a dielectric liquid can be created by unipolar injection that induces EC under the action of the Coulomb force. In the case of a planar electrode geometry, EC presents an analogy with the classical Rayleigh–Benard problem of a horizontal fluid layer heated from below. In both cases, the flow is driven by the body force (thermal buoyancy force for Rayleigh–Benard convection (RBC) and Coulomb force for EC). In the stability analysis, for weak driving forces, both systems remain at rest due to the viscous damping.

Above some critical values, Ra_c and T_c, the flow motion takes place and evolves into a regular pattern of convective cells.

It is well known that the linear bifurcation of RBC is supercritical, while the linear bifurcation of EC is subcritical [4,5]. The subcritical bifurcation was first explained by Felici [6] for weak injection, later for SCL (space-charge-limited) injection in [7] and confirmed experimentally in [8,9]. The subcritical bifurcation is a representative characteristic of EC, featured by a linear stability criterion T_c, a non-linear stability criterion T_f, and a hysteresis loop between these two criteria [8,10]. Recently, Luo et al. showed that a lattice Boltzmann model (LBM) could predict the linear and finite amplitude stability criteria of the subcritical bifurcation in the EC flow [11–13] for both 2D and 3D flow scenarios.

In order to explain the different regimes of instability in a pure EC problem, it is convenient to introduce the electric Nusselt number (*Ne*), which is defined as the ratio of the effective current and the current existing without liquid motion. It can be considered as the analog of the Nusselt number (*Nu*) for a pure thermal problem but has not been studied yet in an ETC problem.

In this article, we consider the convective phenomena in an insulating liquid layer enclosed between two parallel electrodes and subjected to the combined effects of an electric field and a thermal gradient. The effects of both fields simultaneously applied to the fluid layer leads to very complex physical interactions in the flow; these have received much attention by many authors [14–16]. When the space charge only results from ion injection, the coupling between the conservation equations of momentum, electric charge, and energy is ensured via the Coulomb and buoyancy forces. This coupling results from the direct interaction between the velocity, temperature, and charge perturbations as well as from the interaction between the velocity and the electric field. Due to the complexity of the mathematical model, the problem of ETC flows can be investigated mainly by numerical simulations; different methods have been developed and are shown in Refs. [17–20]. For example, an ETHD system with solid–liquid phase change in both rectangular and annular cavities have been analyzed by LBM simulations in Ref. [20]. For SCL injection, EC produces a significant increase in charge transfer [21]. Additional studies on ETHD deal with the evaluation of heat transfer enhancement from numerical [21–24] and experimental [25,26] point of view.

The transition from laminar to chaotic flow in the electro-thermal convection of a dielectric fluid for different Rayleigh numbers Ra was investigated in Ref. [27], using a lattice Boltzmann method. By increasing Ra, the different means of transition to chaos were observed and the chaotic behavior was quantitatively analyzed.

Some preliminary results of electro-thermo-convective flow and its eventual evolution into unsteady and later chaotic flow from the point of view of the electric Nusselt number were obtained in Ref. [28]. Here, we present a detailed and extended study of the behavior of the electric Nusselt number (Ne) on a large time scale as a function of the stability parameter T at various values of the following non-dimensional parameters: $M = 5, 10, 20, 40$; $Ra = 0, 2.10^3, 5.10^3, 10^4$ and for $Pr = 10$. The main purpose of the present study is to explore the subcritical feature of ETC from the point of view of the electrical Nusselt number *Ne* and to investigate the effect of mobility *M* on *Ne*. The entire set of ETC equations is solved by a direct numerical simulation based on the finite volume method [29,30].

2. Statement of the Problem

2.1. Basic Equations and Parameters

We consider an incompressible and perfectly insulating liquid of density ρ, permittivity ε, the ionic mobility K, constant kinematic viscosity v and constant thermal diffusivity κ, enclosed between two parallel planar electrodes of length *L*. The liquid layer of depth *H* is subjected to a potential difference $\Delta V = V_0 - V_1$ and a thermal gradient $\Delta \theta = \theta_1 - \theta_0$ (see Figure 1).
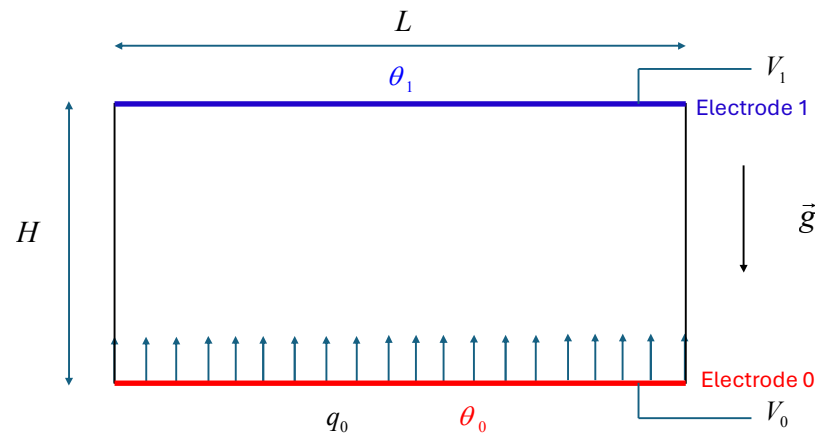
Figure 1. Physical model of ETHD convection in a planar dielectric liquid layer between two parallel electrodes where the lower electrode is a hot ions emitter and the upper one is a collector.

The z-axis is taken perpendicular to the electrodes and the gravity is considered as acting in the negative z-direction. In this study, as the liquid is perfectly insulating, we do not take into account the ion creation due to the dissociation process that can occur in conductive liquids. Here, only the homogeneous and autonomous injection of the unipolar charge at the emitter electrode is considered. This means that $q = q_0$ at $z = 0$ at all times, i.e., that the injector and, therefore, the injection rate are not influenced by the electric field nor by the liquid motion. These injected ions are supposed to have a given ionic mobility K. The lower electrode is chosen as the source of the ions, which are then injected into the fluid and collected at the upper electrode. The liquid is heated from below. The general set of equations for an incompressible fluid expressing the conservation of mass and momentum (Navier–Stokes equations) including electrical and buoyancy effects, the energy balance under Boussinesq assumption, the charge density conservation, Gauss theorem, and the definition of the electric field towards electric potential V, takes the following form:

$$\nabla.\vec{u} = 0 \tag{1}$$

$$\frac{\partial \vec{u}}{\partial t} + (\vec{u}.\nabla)\vec{u} = -\nabla\tilde{p} + \Delta\vec{u} + RTCq\vec{E} + \frac{Ra}{Pr}\theta\vec{e}_z \tag{2}$$

$$\frac{\partial \theta}{\partial t} + \vec{u}.\nabla\theta = \frac{1}{Pr}\Delta\theta \tag{3}$$

$$\frac{\partial q}{\partial t} + \nabla.\left(q(\vec{u} + R\vec{E})\right) = 0 \tag{4}$$

$$\Delta V = -Cq, \quad \vec{E} = -\nabla V \tag{5}$$

where $\vec{u}$ is the velocity, p the static pressure, q the electric charge density in the bulk, $\vec{E}$ the electric field, θ the absolute temperature and V the electric potential, $q\vec{E}$ is the Coulomb force. The following non-dimensional scales are introduced: H for length, the applied voltage $\Delta V = V_0 - V_1$ for electric potential, $\Delta V/H$ for the electric field, q_0 for the charge density, $\varepsilon_0 K\Delta V^2/H^3$ for the current density, v/H for the velocity, $\rho_0 v^2/H^2$ for the pressure, θ for the temperature and H^2/v for time (ρ_0, K_0 and ε_0 are, respectively, the density, the ionic mobility and the permittivity at the reference temperature θ_0).

The system is essentially governed by the following non-dimensional parameters:

$$Ra = \frac{g\beta\Delta\theta\ H^3}{v\ \kappa}, \quad T = \frac{\varepsilon_0\Delta V}{\rho_0 v\ K_0}, \quad C = \frac{q_0 H^2}{\varepsilon_0\Delta V}, \quad M = \frac{1}{K_0}\left(\frac{\varepsilon_0}{\rho_0}\right)^{1/2}, \quad Pr = \frac{v}{\kappa}, \quad R = \frac{T}{M^2},$$

where *Ra* is the Rayleigh number (β thermal expansion coefficient), *T* is the electric instability parameter, defined as the ratio of the driving force and the damping viscous force, *C* is a measure of the injection level (q_0 the injected charge), *g* is the gravity, *Pr* is the Prandtl number, and *R* is the electrical Reynolds number. *M* is the non-dimensional mobility parameter and it only depends on the physical properties of the fluid. The name "mobility", given by Felici in 1969 [6], considering the conversion of the electrical energy ($1/2\varepsilon E^2$) into mechanical energy ($1/2\rho w'$), developed the concept of an electrohydrodynamic mobility ($\varepsilon/\rho)^{1/2}$. Experimental measurements showed that $w' \sim 1/3 \ (\varepsilon/\rho)^{1/2}/E$ [3]. The ratio between the EHD mobility and the true ion mobility K is the parameter *M*; for dielectric liquids its typical values are greater than three [4].

2.2. Initial and Boundary Conditions

The boundary conditions on velocity, temperature, electric potential, and charge density are chosen, as shown in Figure 2. On the horizontal and lateral walls, we apply no-slip boundary conditions. We consider here the fluid initially at rest with simultaneous heating and injection at t = 0.
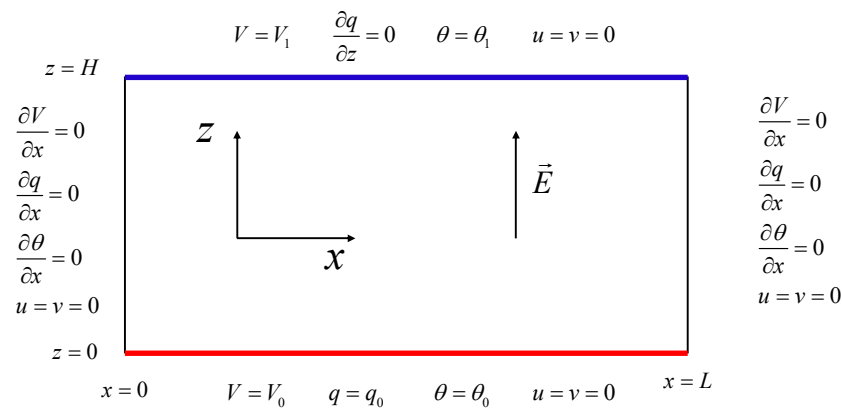

Figure 2. Boundary conditions in the rectangular cavity.

The no-slip condition at the impermeable, thermally, and electrically perfectly conducting electrodes is assumed and the horizontal metallic electrodes are assumed to be rigid. The injection at the emitter is autonomous, which means that the injection rate is not influenced by any perturbation in the bulk and, therefore, that $q = 1$ at z = 0.

2.3. Numerical Method

The set of coupled partial differential Equations (1)–(5) are integrated using the finite volume method [29]. The numerical procedure based on the augmented Lagrangian method. The calculation is fully transient. Special care is taken for the transport Equation (4) for charge density q (because of its hyperbolic nature). The SMART algorithm was utilized in this way.

The boundary condition of the charge density on the collector requires some comments because of the hyperbolic nature of the charge conservation equation. From a mathematical point of view, this implies that a boundary condition on the injector is enough to determine the solution. However, in the numerical procedure, the discretized charge density transport equation involves the value of *q* at some neighboring nodes so that interior nodes next to the boundaries will require the value of *q* at those boundaries. This is where boundary conditions come into play, as they provide pre-defined values of *q* on the boundaries to close the system.

In summary, boundary conditions play a crucial role in solving the charge density transport equation by providing the necessary values of *q* at the boundaries. They ensure the closure of the system and enable accurate modeling and simulation of the behavior of the system near the boundaries. The selection and implementation of appropriate boundary conditions are important considerations in numerical simulations and modeling studies.

The overall algorithm ensures that nothing originates from the collector, which is both physically and mathematically consistent with the principle of the charge conservation equation.

The code has been thoroughly validated and numerical results have been compared with the analytical solution (hydrostatic solution) as well as with some results from linear and non-linear stability analyses [29,30]. Grid independency tests were conducted in order to select the optimal grid to undertake the computation.

3. Results and Discussion

The electro-thermo-convective flow depends on two instability criteria: the Rayleigh number *Ra* and the electrical parameter *T*, as well as on the non-dimensional parameters *Pr* and *M* number. By changing the governing parameters *Ra* and *T*, we investigate the influence of the mobility parameter *M* on the electro-thermo-convective flow from the point of view of the electric Nusselt number. The transition from steady to unsteady flow is also analyzed.

The global effect of convective heat transfer is usually presented by the Nusselt number *Nu*, which is the ratio of the mean heat flux to the flux that would exist without convection for the same temperature difference. In analogy with *Nu*, we introduce the electric Nusselt number *Ne*, given as $Ne = I/I_0$, where *I* is the electric current and I_0 is the electric current without flow motion (note that the current is transported mainly by electro-convection induced by the ion injection from the electrode at $z = 0$ and the dependence between the current *I* and the typical liquid velocity is non-linear).

In this section, we present the electro-thermo-convection (ETC) in the classical geometry of a dielectric liquid layer lying between two parallel planar electrodes and subjected to a strong unipolar injection of charges ($C = 10$). We consider a rectangular cavity of height $H = 1$ and length $L = 2$ in the case of heating and a strong charge injection from the lower electrode. The electric current can be computed by integrating the current density on the entire emitter or the collecting electrodes. Here, *Ne* is calculated on the injecting electrode.

The time evolution of the electrical Nusselt number for the lower instability parameter value ($T = 120$) is given in Figure 3a. At the beginning of the injecting and heating, we observe a brusque increase in the *Ne* number, which reaches an asymptotic value that shows a steady-state behavior. The steady state does not depend on the initial conditions. For $Tc < T < 300$, *Ne* reaches stationary values, whereas for $T > 300$, *Ne* fluctuates around the average values (Figure 3b), which is the sign of the existence of a transition in the flow from a steady laminar regime to an unsteady periodic one.

The flow moves from a motionless state to a convective flow and finally to a periodic one once the system loses its linear stability. This change in regime foreshadows the later appearance of chaotic flow for certain high values of *T*. It can be explained by the fact that the system with higher *T* values *(T > 300)* is essentially in the inertial state of motion and that the flow will probably never reach a steady state.

The results in the next paragraphs are presented for $C = 10$, *Pr* = 10 and for the values of Ra above the critical Rayleigh number ($Ra_c \sim 1708$).
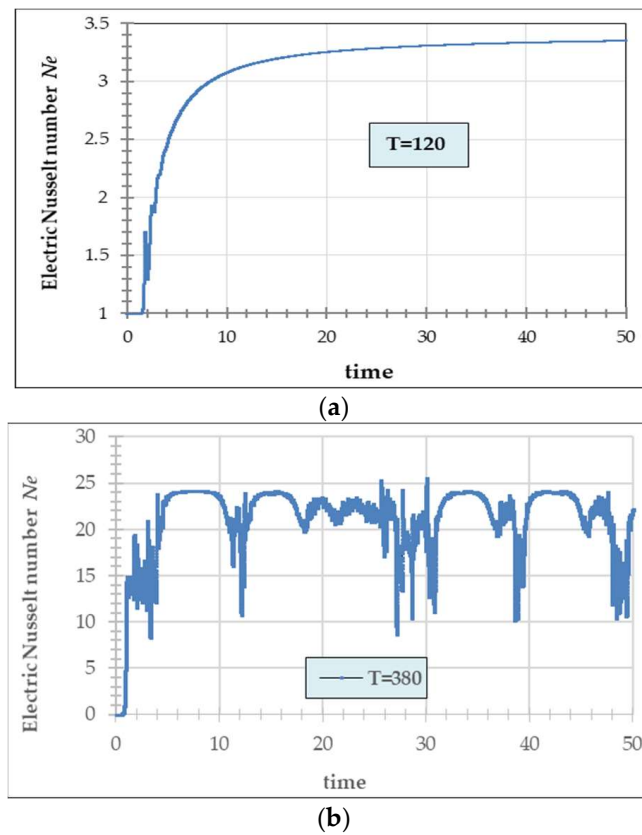
(a)

(b)

Figure 3. Time evolution of electrical Nusselt number for *Ra* = 2000, *Pr* = 10, *M* = 10: (**a**) *T* = 120; and (**b**) *T* = 380.

3.1. Influence of Rayleigh Number Ra on Electric Nusselt Number Ne

Figure 4 shows the evolution of the electric Nusselt number *Ne* with *T* in the case of ETC for different values of the *Ra* number (one is slightly above the critical value *Ra* = 2000 and the others are for higher *Ra* values *Ra* = 5000 and 10,000) and for the pure EC (*Ra* = 0).
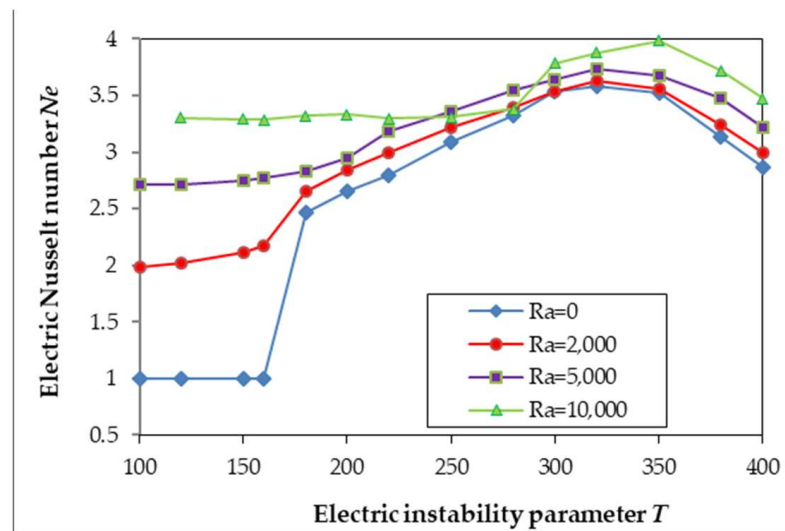
Figure 4. Electric Nusselt number *Ne* with T for *M* = 10, *Pr* = 10, *Ra* = 0 (pure EC), and for different *Ra* numbers.

It can be seen that the Ne number does not depend significantly on the *Ra* number for high enough values of T. We have already demonstrated a similar behavior for the

Nusselt number (Nu) in Refs. [31,32]; for large values of T, the electrical forces dominate the buoyancy forces. In the case of pure EC, when $T < T_c$ (T_c = 163.4 [11]), the perturbation does not trigger the flow instability; the perturbed flow reverses to the hydrostatic state. If T decreases after the EC vortices are formed, they are maintained until $T = T_f$ (T_f = 108.5 [11]), when the system returns to the hydrostatic state. As soon as T is greater than T_c ($T > T_c$) there is a sudden jump in the Ne for EC due to the motion of the liquid initially at rest, with a maximum velocity that exceeds the ion drift velocity. For ETC, when $T < T_c$ we observe greater values for the Ne, which can be explained by the non-linear coupling phenomena between the buoyancy and Coulomb forces; the motion of the liquid induced by thermo-convection drags more electric charge and then causes an increase in the electric current. This means that the increase in the electric Nusselt number Ne is due to thermo-convection. For *Ra* = 2000 and T > 300, the *Ne* values are close to the ones obtained in the case of pure EC. At *Ra* = 10,000 the situation is different; in the initial stage, the flow is thermo-convective with a two-roll structure, (it does not change), but later, at high values of T (T > 280), it changes drastically. There is a jump, and it becomes an electro-thermo-convective flow structure with four rolls.

3.2. Influence of Mobility Parameter M and T

In this section, we study the electro-thermo-convection driven by buoyancy and Coulomb forces for a large set of *M* parameter values. Numerical simulations are made for larger values of *T* to those corresponding with the saturation zone and to the fully developed turbulence flows. Figure 5 presents the variation in the electric Nusselt number *Ne* as a function of *T* under different mobility parameters.
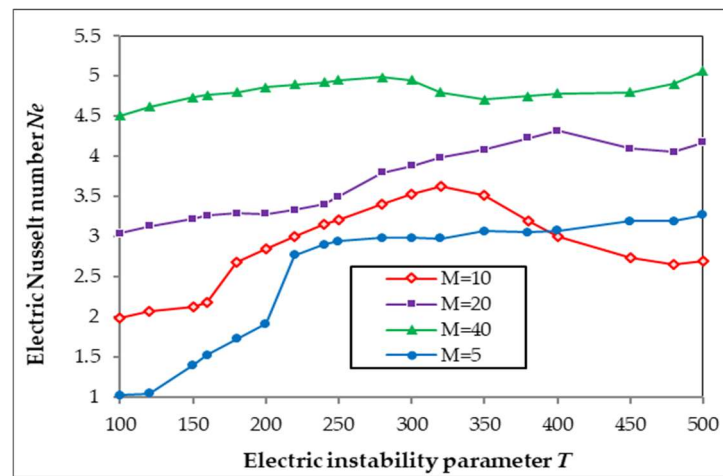

Figure 5. Electric Nusselt number *Ne* with *T* for *Ra* = 2000, *Pr* = 10, and mobility parameters M = 5, 10, 20, 40.

The shape of the curve for *M* = 5 is similar to those obtained in Ref. [9] for pure electro-convection; *Ne* grows with *T* then reaches its saturation value. For other values of *M*, we can see that *Ne* increases with *T* until *T*~350 but does not reach the saturation value because of the influence of thermo-convection. For high values of *T* (*T* > 350), *Ne* decreases due to the transition from viscous to non-linear flow. For a high value of *M* (*M* > 40), i.e., liquids with very low ion mobility, the influence of *T* seems less important and the flow remains thermo-convective. For higher values of *T* (*T* > 450), *Ne* increases again. The increases in velocity and turbulent mixing can explain this.

In Figure 6, the variation of the electric Nusselt number *Ne* with *M* is presented for different values of the instability criteria *T*. We can see the fast linear growth of *Ne*, which is similar to the results obtained in Ref. [9].
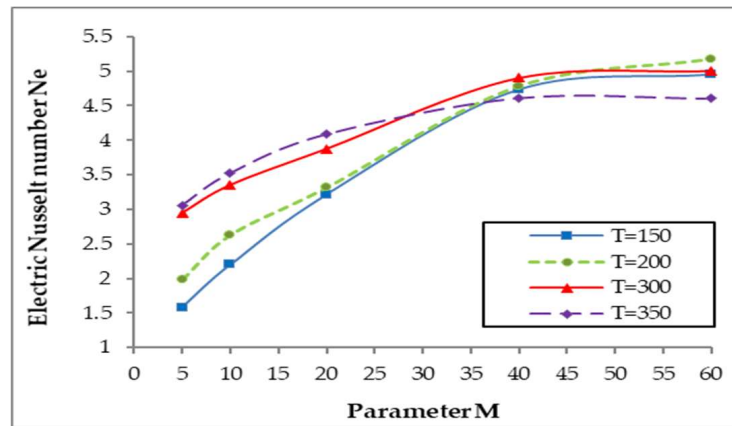
Figure 6. Electric Nusselt number *Ne* with *M* for different values of instability parameter *T*; *Pr* =10 and *Ra* = 2000.

Fom theoretical predictions and experimental observations [9], the saturation value of Ne depends on the physical property of the liquids and is given as a function of parameter M by the following expression:

$$Ne = \frac{I}{I_0} \approx \left(\frac{M}{3} \right)^{1/2} \tag{6}$$

Figure 7 presents the numerical results for the saturation value of *Ne* taken from Figure 5 and those obtained from formula (6) for pure electrohydrodynamic problems [9]. As one can see, the shape of both curves is similar, the difference between them being due to the influence of thermo-convection.
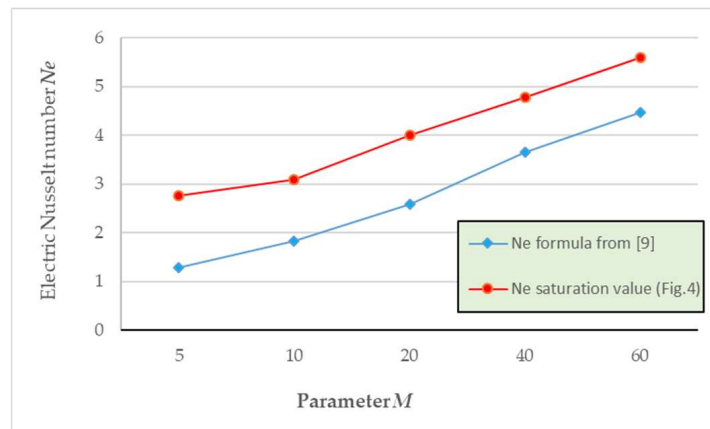

Figure 7. Electric Nusselt number *Ne* for several values of *M*; curve in blue corresponds to formula (6) [9]; *Ne* values of the red curve are taken at the saturation point of Figure 5.

3.3. Flow Transition Process Described by the Maximum Fluid Velocity

Figure 8 presents the bifurcation diagram for thermo- and electro-convection expressed with the maximum fluid velocity in the bulk V_{max} versus *T* for different values of parameter *M*. Initially, V_{max} increases slowly with *T*. Then, for certain values of *T*, the slope of the curve changes and continues to increase. The change in slope depends on the values of *M* and corresponds to the transition from thermo- to electro-convection. For smaller values of *M* (*M* = 5 and *M* = 10, see Figure 8a), the values of V_{max} are much higher than for the other represented *M* (see Figure 8b), but the behavior of the curves is similar.
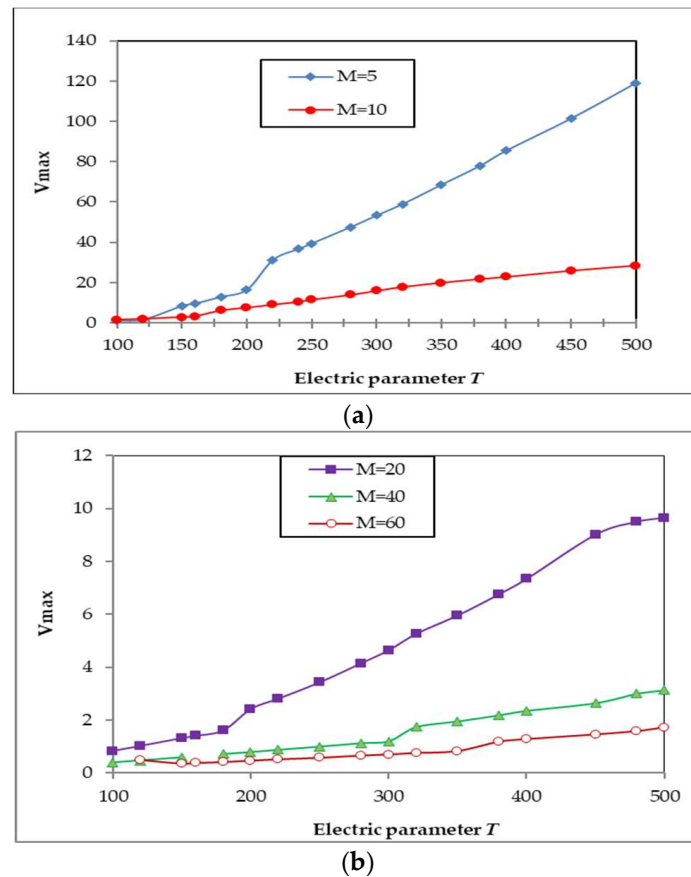
(**a**)

(**b**)

Figure 8. Maximum velocity with T for Pr = 10 and different values of M: (**a**) M = 5, M = 10; and (**b**) M = 20, 40, and 60.

Figure 9 shows the evolution of the maximum velocity magnitude in time for different driving parameters *M* and *T* and *Ra* = 2000 and *Pr* = 10. Figure 9a plots the velocity magnitude for *M* = 10 and three different electric Rayleigh numbers, *T* = 150, 220 and 380. For *T* = 150 the flow remains inactive at the early stage; the velocity magnitude then grows quickly with an exponentially growing rate. Finally, the system reaches a steady state with two thermo-convective roll patterns. The curve for *T* = 220 has a slightly different behavior; it first develops as for *T* = 150 but after a certain time (~10) there is a sudden upward jump and it reaches a steady state with four convective cells. This means that the electro-convection dominates, but the flow rests in a steady state. For *T* = 380, the *Vmax* curve grows rapidly; the flow becomes strongly unsteady and looks periodic.

Figure 9b depicts the evolution in time of the maximum velocity magnitude at different settings of the driving parameters M and T corresponding to the values at which the slopes of the curves change (see Figure 8). The evolution of peak velocity Vmax also experiences two different stages after the initial disturbance. The first one is the exponential growth stage, which is the same for the smaller values of T (see Figure 9a). However, the second stage is quite different; Vmax grows rapidly, the flow becomes strongly unsteady and looks chaotic. In simpler terms, the flow transitions from a stationary state to a thermo-convective flow, followed by an electro-convective flow, and eventually reaches a chaotic state once the system loses its linear stability. This means that the system with high T is essentially in the inertial state of motion. Due to the electric force and destabilizing buoyancy force, the system exhibits electro-thermo-convective vortices and transitions to a chaotic flow field, where the flow fluctuates irregularly in time.
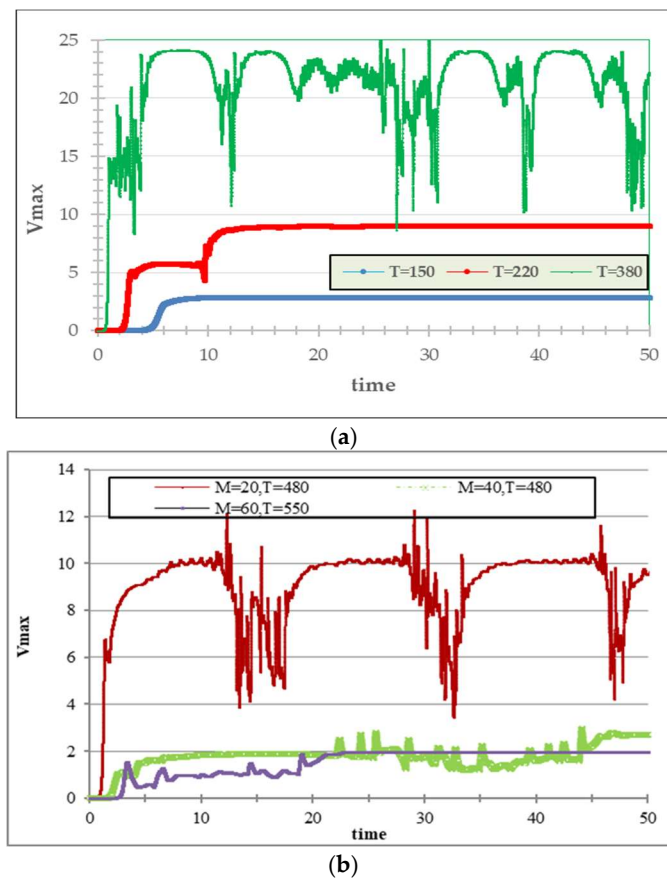
(**a**)

(**b**)

Figure 9. Time evolution of the maximum velocity magnitude for Ra = 2000, Pr = 10: (**a**) for M = 10; T = 150, 220 and 380; and (**b**) electro-thermo-convection at different driving parameters *M* and *T* in an unsteady regime.

In Figure 10, we present the charge density distribution and the stream function at a steady convective state for the values of the electrical instability parameters *T*, in which the flow passes from a thermo-convective pattern with two rolls to an electro-convective one with four rolls.

(**a**)   (**b**)
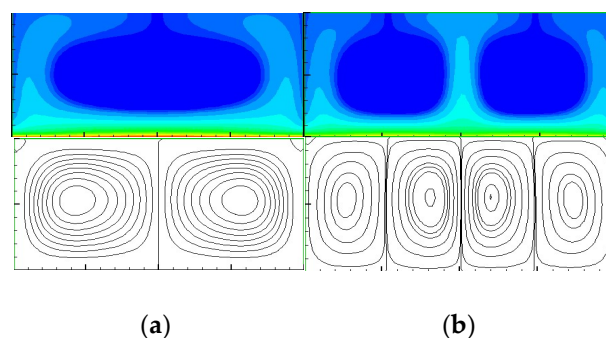
Figure 10. Distributions of charge density and stream function at a steady convective state for Ra = 2000, Pr = 10: (**a**) T = 200 with two thermo-convective rolls; and (**b**) T = 220 with four electro-convective rolls.

In Figure 10, we can observe the formation of electro-convective cells with charge-depleted central regions. This absence of charges in the core of the cell is a consequence of the non-uniform distribution of the electric field and the rotational fluid motion induced by the Coulomb force. This well-established phenomenon is a hallmark of Coulomb-driven

electro-convective flows and has been consistently reported in numerous experimental and numerical investigations [4,5,12,30].

In Figure 11, the transition from a thermo- to an electro-convective regime is shown in detail by the stream function. For M = 5 we see that the two-roll patterns for T < T$_c$ change to four-roll patterns from T = 220, as in the pure electro-convective case. The same change in the roll patterns also occurs for M = 10, when four rolls appear at T approximatively equal to 220 and for M = 20, in which the change appears at T = 250. For M = 40 and M = 60, the two-roll pattern turns to a four-cell one at a higher level of T—T~320, and T~380, respectively.
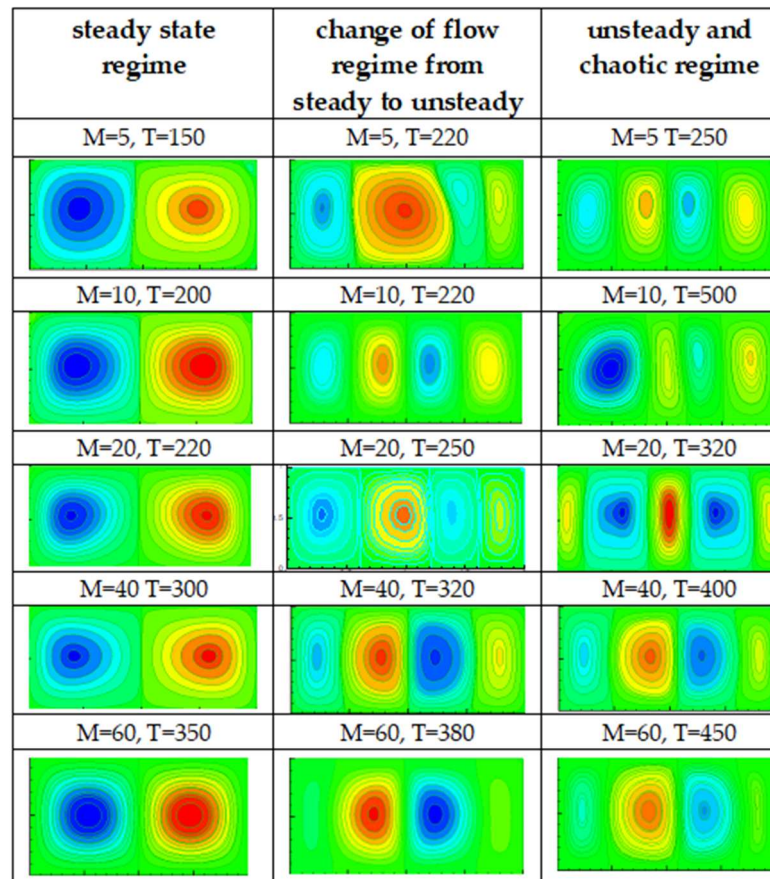

Figure 11. The stream function in electro-thermo-convection for different parameters *M* and *T*, *Ra* = 2000, *Pr* = 10.

The change in the number of rolls corresponds to a change in the slope of the curve (see Figures 8 and 9a for *T* = 150 and 220). In all cases, the change in the slope of the curves *Ne*(*T*) always occurs when the number of rolls passes from two to four; in all cases *Ne* seems to saturate for the highest values of *T*. Such a transition from two to four convective cells has already been observed [31,32] in another study. We must also note that a change from two to four cells for *M* > 40 appears for higher values of *T*, which means that the flow remains thermo-convective up to *T* > 320. In the last column, the patterns are already in an unsteady and chaotic regime.

4. Conclusions

This work presents a numerical study of electro-thermo-convective phenomena in an insulating liquid layer between two parallel plates from the point of view of the electric Nusselt number. Numerical simulations for a large range of *M* and *T* values corresponding to the saturation zone and a fully developed chaotic flow were performed. It was confirmed once again that electrical forces dominate buoyancy forces as far as *T* > *T$_c$*. For higher

values of *T*, and for a fixed *M*, the change in the number of rolls has an influence on the shape of the *Ne*(*T*) curves. It can be clearly seen that when the number of rolls changes, the slope of the maximum velocity with *T* changes as well. The transition from thermal to electro-convective flow was found and studied. We show the transition from thermo- to electro-convective flow, and, later, to unsteady flow as a function of parameter *M* and *T* through the maximum fluid velocity. For lower values of *M* (*M* = 5 and *M* = 10), electro-convection dominates for the values of *T* close to the linear instability criteria and *Ne*(*T*) grows fast. For high values of *M*, the electrical forces exceed the buoyancy forces for high *T* values. When *T* reaches the region in which the convective flow moves to the inertial state of motion and finally to chaos, *Ne* increases with *T* for a fixed *M*. Some of the results on *Ne* obtained here are in good agreement with the results presented in Ref. [9].

References

1. Castellanos, A. *Electrohydrodynamics*; Springer: Berlin/Heidelberg, Germany, 1998.
2. Atten, P.; Cluskey, F.M.; Perez, A.T. Electro-convection and its effect on heat transfer. *IEEE Trans. Electr. Insul.* **1988**, *23*, 659–667. [CrossRef]
3. Cluskey, F.M.; Atten, P.; Perez, A.T. Heat transfer enhancement by electro-convection resulting from an injected space charge between parallel plates. *Int. J. Heat Mass Transf.* **1991**, *34*, 22–37.
4. Atten, P. Electrohydrodynamic instability and motion induced by injected space charge in insulating liquids. *IEEE Trans. Dielectr. Electr. Insul.* **1996**, *3*, 1–17. [CrossRef]
5. Castellanos, A. Coulomb-driven convection in electrohydrodynamics. *IEEE Trans. Electr. Insul.* **1991**, *26*, 1201–1215. [CrossRef]
6. Felici, N.D. Conduction in liquid dielectrics (partII): Electrohydrodynamic phenomena. *Direct Curr.* **1972**, *147*, 147–165.
7. Atten, P.; Lacroix, C.J. Non linear hydrodynamic stability of liquids subjected to unipolar injection. *J. Mec.* **1979**, *18*, 469–510.
8. Atten, P.; Lacroix, J.C. Electrohydrodynamic stability of liquids subjected to unipolar injection: Non linear phenomena. *J. Electrost.* **1978**, *5*, 439–452. [CrossRef]
9. Lacroix, J.C.; Atten, P.; Hopfinger, E.J. Electro-convection in a dielectric liquid layer subjected to unipolar injection. *J. Fluid Mech.* **1975**, *69*, 539–563. [CrossRef]
10. Luo, K.; Wu, J.; Yi, H.-L.; Liu, L.-H.; Tan, H.-P. Hexagonal convection patterns and their evolutionary scenarios in electro-convection induced by a strong unipolar injection. *Phys. Rev. Fluids* **2018**, *3*, 053702. [CrossRef]
11. Luo, K.; Wu, J.; Yi, H.-L.; Tan, H.-P. Lattice Boltzmann model for Coulomb-driven flows in dielectric liquids. *Phys. Rev. E* **2016**, *93*, 023309. [CrossRef]
12. Luo, K.; Wu, J.; Yi, H.L.; Tan, H.P. Lattice Boltzmann modelling of electro-thermo-convection in a planar layer of dielectric liquid subjected to unipolar injection and thermal gradient. *Int. J. Heat Mass Transf.* **2016**, *103*, 832–846. [CrossRef]
13. Luo, K.; Wu, J.; Yi, H.-L.; Tan, H.-P. Three-dimensional finite amplitude electroconvection in dielectric liquids. *Phys. Fluids* **2018**, *30*, 023602. [CrossRef]
14. Pontiga, F.; Castellanos, A. Physical mechanism of instability in a liquid layer subjected to an electric field and a thermal gradient. *Phys. Fluids* **1994**, *6*, 1684–1701. [CrossRef]
15. Laohalertdecha, S.; Naphon, P.; Wongwisesb, S. A review of electrohydrodynamic enhancement of heat transfer. *Renew. Sustain. Energy Rev.* **2007**, *11*, 858–876. [CrossRef]
16. Léal, L.; Miscevic, M.; Lavieille, P.; Amokrane, M.; Pigache, F.; Topind, F.; Nogarèdec, B.; Tadrist, L. An overview of heat transfer enhancement methods and new perspectives: Focus on active methods using electroactive materials. *Int. J. Heat Mass Transf.* **2013**, *61*, 505–524. [CrossRef]
17. Pontiga, F.; Castellanos, A. The onset of electrothermal convection in non polar liquid layers on the basis of dissociation-injection conductivity model. *IEEE Trans. Ind. Appl.* **1992**, *28*, 520–527. [CrossRef]

18. Pontiga, F.; Castellanos, A. Galerkin analysis of electro-thermal instabilities in plane liquid layers. *IEEE Trans. Ind. Appl.* **1994**, *30*, 862–876. [CrossRef]
19. Lu, Z.; Liu, G.; Wang, B. Flow structure and heat transfer of electro-thermo-convection in a dielectric liquid layer. *Phys. Fluids* **2019**, *31*, 064103. [CrossRef]
20. Lu, C.-L.; Luo, K.; Zhou, P.-C.; Yi, H.-L. Lattice Boltzmann analysis for electro–thermo–convection with a melting boundary in horizontal concentric annuli. *Phys. Fluids* **2021**, *33*, 043605. [CrossRef]
21. Karayiannis, A.T. Electrohydrodynamic enhancement of heat transfer and fluid flow. *Heat Recov. Syst. CHP* **1995**, *15*, 389–423.
22. Hassen, W.; Borjini, M.N.; Aissia, H.B. Enhanced heat transfer by unipolar injection of electric charges in differentially heated dielectric liquid layer. *Fluid Dyn. Mater. Process.* **2012**, *8*, 381–395.
23. Hassen, W.; Kolsi, L.; Oztop, H.F.; Al-Rashed, A.A.A.; Borjini, M.N.; Al-Salem, K. Electro-thermo-capillary-convection in a square layer of dielectric liquid subjected to a strong unipolar injection. *Appl. Math. Model.* **2018**, *63*, 349–361. [CrossRef]
24. Wu, J.Z.; Wang, B.F.; Lu, Z.-M.; Zhou, Q. The heat transfer enhancement by unipolar charge injection in a rectangular Rayleigh–Bénard convection. *AIP Adv.* **2022**, *12*, 015212. [CrossRef]
25. Mirzaeia, M.; Saffar-Avvalb, M. Enhancement of convection heat transfer using EHD conduction method. *Exp. Therm. Fluid Sci.* **2018**, *93*, 108–118. [CrossRef]
26. Gao, M.; Zhang, L.-S.; Zhang, D.; Zhang, L.-X. Experimental study on the enhancement of free convection heat transfer under the action of an electric field. *Exp. Therm. Fluid Sci.* **2019**, *104*, 9–14. [CrossRef]
27. Li, T.F.; Su, Z.G.; Luo, K.; Yi, H.L. Transition to chaos in electro-thermo-convection of a dielectric liquid in a square cavity. *Phys. Fluids* **2020**, *32*, 013106. [CrossRef]
28. Koulova, D.; Traoré, P.; Romat, H. Effect of Electric Nusselt number on Electro-Thermo-Convection in dielectric liquid subjected to unipolar injection. In Proceedings of the IEEE 20th International Conference on Dielectric Liquids (ICDL), Roma, Italy, 23–27 June 2019.
29. Traoré, P.; Perez, A.; Koulova, D.; Romat, H. Numerical modeling of finite amplitude subjected to both unipolar injection and temperature gradient. *J. Fluid Mech.* **2010**, *658*, 279–293. [CrossRef]
30. Traoré, P.; Perez, A. Two-dimensional numerical analysis of electroconvection in a dielectric liquid subjected to strong unipolar injection. *Phys. Fluids* **2012**, *24*, 037102. [CrossRef]
31. Koulova, D.; Traoré, P.; Romat, H.; Wu, J.; Louste, C. Numerical simulations of Electro-Thermo-Convection and Heat Transfer in 2D cavity. *J. Electrost.* **2013**, *71*, 341–344.
32. Koulova, D.; Traoré, P.; Romat, H. Numerical Study of the heat transfer and electro-thermo-convective flow patterns in a dielectric liquid layer subjected to unipolar injection. *J. Electrost.* **2013**, *71*, 970–975.